NJC

PAPER

View Article Online
View Journal | View Issue

Cite this: *New J. Chem.*, 2018, **42**, 4192

One-pot synthesis of microporous nanoscale metal organic frameworks conjugated with laccase as a promising biocatalyst†

Arpita Samui and Sumanta Kumar Sahu *

Enzymes immobilized into or onto a smart material have attracted much attention due to their numerous applications as biocatalysts. Recently, microporous metal organic frameworks (MOFs) have been used as active supports for enzyme immobilization owing to their high surface area, high porosity, and tunable functionality. However, challenges remain in the development of MOFs for enzyme immobilization regarding (i) green synthesis approaches, (ii) high loading and activity efficiency, (iii) facile immobilization processes, and (iv) obtaining stable enzyme activity. In this study, we have developed amine-functionalized nanoscale metal organic framework (NMOF) NH_2-MIL-53(Al) as a support for enzyme immobilization using green synthesis in a one-pot procedure. Herein, laccase is immobilized into the NMOFs, which possess highest stability and activity at pH 4–6, using a coprecipitation method. As most reported MOFs are unstable under slightly acidic conditions, developing MOFs that are stable at low pH is challenging. After successful immobilization, it is observed that 625 mg laccase is immobilized per 1 g of NMOF. Importantly, the immobilized enzyme showed good reusability, retaining 63% of its initial activity after being reused 10 times. Our study highlights the development of NMOFs that contain more laccase and retain stability and activity and.

Received 21st September 2017,
Accepted 5th February 2018

DOI: 10.1039/c7nj03619a

rsc.li/njc

1. Introduction

Enzyme immobilization has received considerable attention in recent years regarding applications in industrial biocatalysis.[1–3] Immobilization can improve the stability and catalytic activity of enzymes, and facilitate their recovery and reuse. Many conventional supports have been developed for enzyme immobilization, including microparticles, silica gel, hydrogels, and porous materials.[4–7] To improve enzyme immobilization, research has focused on developing suitable supports by adjusting different parameters, such as particle size, shape, porosity, surface area, surface charge, surface chemistry, and roughness. However, an ideal support to meet all requirements for efficient enzyme immobilization has yet to be obtained owing to their structures and surface properties.

Metal organic frameworks (MOFs) are inorganic–organic hybrids comprising metal ions or clusters coordinated with multidentate organic ligands to construct one-, two-, or three-dimensional crystalline structures. Owing to their unique properties, such as well-defined pore structures with large surface areas, high porosity, tunable pore sizes, and suitable thermal stability, MOFs have been extensively studied for diverse applications, such as gas storage/separation, sensing, catalysis, and drug delivery.[8–12] Recently, MOFs have been applied as promising materials for enzyme immobilization.[13,14] In the last two years, many research groups, including ourselves, have explored the immobilization of enzymes, including lipase,[15,16] hydrolase,[17] urate oxidase,[18] glucose oxidase,[19] catalase,[20] urease,[21] and laccase,[22] into different MOFs. The resulting enzyme–MOF composites exhibit excellent stability and activity due to the enzyme protection afforded by the frameworks. In particular, recent reports have shown that enzymes can be directly immobilized during MOF crystal formation in a one-step synthesis. For example, Hou *et al.* prepared glucose oxidase-embedded mZIF-8 in one step,[23] Wu *et al.* synthesized ZIF-8 embedded with multiple enzymes (glucose oxidase and horseradish peroxidase) under mild conditions,[24] and Nadar *et al.* immobilized glucoamylase into ZIF-8 in a one-step synthesis.[25] Although these strategies are promising approaches to enzyme immobilization into controlled MOF structures and morphologies, further development is required to produce new biocatalysts.

Laccase (E.C.1.10.3.2, *p*-benzenediol: oxygen oxidoreductase) is a multicopper oxidase that can oxidize a large number of organic and inorganic substrates, particularly phenols and aromatic amines. Laccase has been used in biosensors, biofuel cells, effluent treatment, and a variety of other applications.[26–29]

Department of Applied Chemistry, Indian Institute of Technology (ISM), Dhanbad 826004, Jharkhand, India. E-mail: sksahu@iitism.ac.in, sumantchem@gmail.com; Fax: +91 326-2307772; Tel: +91 326-2235936

† Electronic supplementary information (ESI) available. See DOI: 10.1039/c7nj03619a

In its native form, laccase application is restricted due to high production costs, low operational stability, and unfavorable recoverability. Laccase immobilization on solid supports can efficiently overcome these disadvantages and has, therefore, received significant attention. Various materials, including chitosan-modified alginate beads,[30] titania nanoparticles,[31] magnetic SiO_2,[32,33] amine-functionalized Fe_3O_4@C nanoparticles,[34] and EDTA–Cu(II) chelating magnetic nanoparticles,[35] have been used for laccase immobilization and their properties investigated. Among these reported materials, laccase is generally immobilized through tedious multistep approaches. However, developing a smart support that can be synthesized with laccase immobilization in one pot remains a significant challenge. Many researchers have reported that laccase possesses higher activity and stability under acidic conditions (*i.e.*, pH 4–6).[36,37] Therefore, support materials that are stable in this pH range could be significant for the stabilization and activity performance of immobilized laccase. In this context, MOFs with ordered microporous structures, in which enzyme molecules can be homogeneously dispersed within the framework, may be ideal supports for laccase immobilization. However, few reports exist regarding laccase immobilization on MOFs. For example, Pang *et al.* developed bimodal mesoporous Zr-MOF for laccase immobilization *via* adsorption.[22] Simultaneously, Zhong *et al.* synthesized mesoporous Cu-MOF for laccase immobilization.[38] However, in all of these reports, MOF stability at pH 4–6 was a major issue. In this study, we aimed to prepare alternative MOFs with high laccase loadings that are acid-stable in a one-pot synthesis.

Herein, we have fabricated amine-functionalized supports (NH_2-MIL(53)-Al) with laccase immobilization using a one-pot method. The MOF synthesis and enzyme immobilization processes are shown in Scheme 1. The loading capacity and activity of immobilized laccase on these MOFs were compared with those of native laccase under different thermal and pH conditions. Immobilization on the MOF support was facile without modification and the immobilized laccase possessed high catalytic activity, stability, and reusability.

2. Materials and methods

2.1. Materials

Anhydrous aluminum chloride powder ($AlCl_3$, 99%) and 2-amino-terephthalic acid (NH_2-BDC) were purchased from Alfa Aesar. Sodium hydroxide pellets (NaOH) were purchased from Rankem. Laccase (EC 1.10.3.2, *p*-benzenediol: oxygen oxidoreductase) from Trametes versicolor (powder, light brown, ≥ 0.5 U mg^{-1}) and 2,2′-azino-bis(3-ethylbenzothiazoline-6-sulfonic acid) diammonium salt (ABTS, $\geq 98\%$ by HPLC) were purchased from Sigma Aldrich Chemicals, USA. For sodium acetate buffer preparation, sodium acetate trihydrate ($CH_3COONa{\cdot}3H_2O$) was purchased from Rankem and glacial acetic acid (CH_3COOH) was purchased from Fisher Scientific. Millipore water was used for all reactions.

2.2. Synthesis of NMOFs (NH_2-MIL-53(Al))

Nanoscale metal–organic framework NH_2-MIL-53(Al) was prepared in water at room temperature using the procedure of M. Sánchez-Sánchez *et al.*[39] Solution 1 was prepared by dissolving NH_2-BDC (75.12 mg, 0.253 mmol) and NaOH (28 mg, 0.7 mmol) in distilled water (4 mL) with magnetic stirring at 400 rpm. Solution 2 was prepared by dissolving $AlCl_3$ (100 mg) in distilled water (4 mL). Solution 2 was added dropwise to solution 1 with stirring and a yellow solid formed immediately. After stirring for 12 h, the product was separated from the reaction mixture by centrifugation and washed three times with distilled water. The synthesized NMOF was dried at 55 °C in a vacuum oven and characterized.

2.3. One-pot synthesis of NMOF-immobilized laccase [NH_2-MIL-53(Al)/laccase]

For the one-pot immobilization of laccase into NMOFs, NH_2-MIL-53(Al) was prepared using the procedure described above. Solutions 1 and 2 were prepared as above, with solution 2 added dropwise to solution 1 with stirring. After stirring for 1 h, a fixed amount of laccase (100 mg) in distilled water (6 mL) was added dropwise to the mixture and stirred for a further 12 h. The resultant yellow product was separated from the reaction mixture

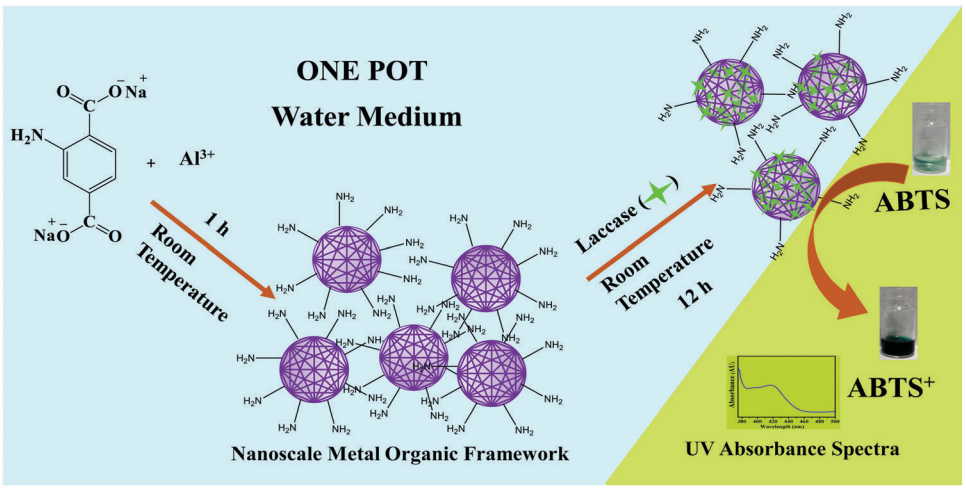

Scheme 1 Laccase immobilization into NMOFs using a one-pot synthesis.

by centrifugation and washed three times with distilled water. Some of the product was stored at 4 °C to maintain laccase activity, while residual product NH_2-MIL-53(Al)/laccase was dried at 55 °C in a vacuum oven for further characterization.

2.4. Laccase activity assay

The activities of free and immobilized laccase were determined using ABTS as substrate. First, ABTS solution (15 mM) was prepared by dissolving ABTS (82.305 mg) in distilled water (10 mL). The activities of free and immobilized laccase were determined using the assay described by Li *et al.*[40,41] Briefly, ABTS solution (0.1 mL) was added to sodium acetate buffer (2.9 mL, pH ~ 4.6) containing a certain amount of free and immobilized laccase. The mixture was stirred gently for 5 min and then absorbance was measured using a UV-visible spectrophotometer at 420 nm.

2.5. Kinetic study (K_m & V_{max})

Kinetics parameters for free and immobilized laccase were determined by varying the substrate concentrations from 0.5 mM to 1.0 mM in acetate buffer solution (pH ~ 4.6) at 25 °C. Kinetic parameters, such as the Michaelis–Menten constant (K_m) and maximum rate of reaction (V_{max}), were calculated from the Lineweaver–Burk plot:[38,40]

$$\frac{1}{V} = \frac{1}{V_{max}} + \frac{K_m}{V_{max}}\frac{1}{[S]} \quad (1)$$

where [S] is the substrate (ABTS) concentration and V is the reaction rate. The plot of $\frac{1}{V}$ *vs.* $\frac{1}{[S]}$ was linear. V_{max} was obtained from the intercept and K_m was calculated from the slope.

2.6. Effects of pH and temperature

The effect of pH on free and immobilized laccase was assessed by measuring the enzyme activity in acetate buffer at different pH values (pH 3–7) at room temperature. Free and immobilized laccase were placed in each solution with different pH values for 30 min and enzymatic activities were determined using the activity assay described above.

The effect of temperature on free and immobilized laccase in acetate buffer (pH ~ 4.6) was also assessed at different temperatures, ranging from 30 to 90 °C. Free and immobilized laccase were exposed to each temperature for 30 min and enzyme activity was determined using the activity assay described above.

2.7. Stability study

The thermal stabilities of free and immobilized laccase were assessed in acetate buffer solution (pH ~ 4.6). Solutions of free and immobilized laccase were heated on a water bath at 60 °C and enzyme activity was determined at 30 min intervals for 3 h. The activities of both free and immobilized laccase were then compared with the initial solution, which was considered to have 100% activity.

The stability of immobilized laccase was assessed during storage for seven weeks. Immobilized laccase was centrifuged from the reaction mixture, washed several times with distilled water, and then stored at 4 °C. The activity was examined at 7 day intervals in acetate buffer solution. Finally, the activities were compared with the initial activity (first day activity, considered 100% activity) using the activity assay.

The reusability of the immobilized enzyme was assessed to determine its operational stability by recycling the same immobilized enzyme in acetate buffer solution at room temperature. After each use, the immobilized laccase was separated from the reaction mixture, washed with distilled water, and reused for activity determination. Finally, the activities were compared with the initial activity (considered 100% activity).

2.8. Study of loading capability

To evaluate the loading capability of enzymes into the NMOFs, different amounts of laccase were used in the one-pot synthesis. Firstly, solutions 1 and 2 were prepared by dissolving NH_2-BDC (37.56 mg) with equivalent amounts of NaOH (14 mg) and $AlCl_3$ (50 mg) in water, respectively. Solution 2 was then added to solution 1 with stirring. Different amounts of laccase (10, 20, 30, 40, and 50 mg) in distilled water (4 mL) were added to each experiment. The activity of the product from each experiment was then determined from absorbance using the ABTS activity assay.

2.9. Characterization

The morphologies of NMOF and laccase-immobilized NMOFs were investigated by field-emission scanning electron microscopy (FESEM) analysis using a Supra 55 instrument with an airlock chamber. The average hydrodynamic particle size was analyzed using dynamic light scattering (DLS) techniques (SZ-100 instrument, Horiba Scientific, Japan). Surface functional groups were investigated using Fourier transform infrared spectroscopy (FTIR; Thermo Nicolet Nexus FTIR (model 870)) at room temperature with a scanning range of 400–4000 cm^{-1} using the KBr pallet technique. The phase structure and crystal morphology were determined by powder X-ray diffraction (XRD) using an Expert Pro (Philips) X-ray diffractometer with Cu Kα radiation. Thermogravimetric analysis (TGA) of the NMOF and NMOF–laccase composite was conducted using an SDTQ600 thermogravimetric analyzer (TA instruments) under N_2 from 50 to 900 °C at a rate of 10 °C min^{-1}. The surface area and pore size distribution of the NMOF and NMOF–laccase composite were determined using a microporous Brunauer–Emmett–Teller (BET) surface area analyzer (Quantachrome Instruments). Laccase activity was detected by UV-vis spectroscopy using a Shimadzu UV-1700 spectrophotometer.

3. Results and discussion

Herein, we have developed a one-pot synthetic procedure for laccase immobilization into NMOFs. NH_2-MIL-53(Al) NMOF was chosen as the support owing to its good stability at low pH, maximal laccase immobilization on the NMOF surface, and good storage stability after enzyme immobilization.

3.1. Surface morphology & particle size analysis

The surface morphology of NH_2-MIL-53(Al) and the extent of one-pot laccase immobilization were determined using FESEM,

as shown in Fig. 1(a) and (c). Laccase immobilization into the NMOFs had no effect on the surface morphology. The NMOF particle size was about 30–40 nm and remained similar after laccase immobilization. Furthermore, DLS analysis was conducted for the NMOF and NMOF–laccase composite, as shown in Fig. 1(b) and (d), respectively. The DLS study showed that the hydrodynamic diameter of the NMOF was 101 nm, while that of the NMOF–laccase composite was 134 nm. This increase might be due to enzymes being immobilized both on the outer NMOF surface and inside the NMOF framework. However, DLS showed one conflicting result, with the particle size of both the NMOF and NMOF–laccase composite larger than those observed by FESEM. This might be due to NMOF agglomeration and particle swelling in the water medium.[42] DLS measurements show the average hydrodynamic particle diameter rather than the actual size, which might explain the increased particle size compared with those measured by FESEM.

To study the effect of laccase immobilization on the NMOF morphology, NH_2-MIL-53(Al)/laccase was prepared using different amounts of laccase (20, 30, 40, and 50 mg). FESEM images of the resultant NH_2-MIL-53(Al)/laccase composited are shown in Fig. S1 (ESI†). These FESEM images confirmed that there was no change in the surface morphology during laccase immobilization into the NMOF and that the particle size remained almost the same.

3.2. FTIR analysis

Laccase immobilization into NH_2-MIL-53(Al) in the one-pot procedure was examined by surface functional group analysis using FTIR spectroscopy. FTIR spectra of laccase, NMOF, and NMOF–laccase composite are shown in Fig. 2a. The NMOF peak at 3656 cm^{-1} was attributed to bridging –OH groups,[43] while peaks at 3500 cm^{-1} and 3385 cm^{-1} were attributed to $-NH_2$ groups.[43,44] Peaks in the region 1200–1700 cm^{-1} were attributed to Al-coordinated carboxylate groups.[44] Furthermore, bands at around 1700 and 1500 cm^{-1} were attributed to asymmetric stretching of carbonyl groups, while bands at around 1440 and 1400 cm^{-1} were assigned to symmetric stretching of carbonyl groups. For laccase, the band observed at 3680–3000 cm^{-1} was due to –OH and –NH bonds, while the peak at 2920 cm^{-1} was due to C–H stretching in CH_2 groups present in laccase protein.[45,46] Other characteristic protein peaks were also present in laccase.[46–48] For example, the spectrum also showed an amide I band at 1642 cm^{-1} due to C═O stretching, an amide III band around 1420–1210 cm^{-1} due to CN stretching and NH bending, amide V and VI bands at 800–500 cm^{-1} due to out of plane NH and C═O bending, and a band at 1165–948 cm^{-1} characteristic of protein in laccase. The FTIR spectrum of NH_2-MIL-53(Al)/laccase after one-pot immobilization showed that all characteristic peaks of laccase and the NMOF were present. Magnified images of the FTIR spectra are shown in Fig. S2 (ESI†). A broad band observed at 3720–3000 cm^{-1} was due to overlap of the corresponding bands in laccase (for –OH and –NH bonds) and NH_2-MIL-53(Al) (for bridging –OH and NH_2 groups). A slightly broad band was also observed at around 2920 cm^{-1} due to $-CH_2$ groups in laccase. The NMOF peaks in the region 1700–1200 cm^{-1} were also present after laccase immobilization. However, some NMOF peaks were slightly broader in NH_2-MIL-53(Al)/laccase due to the presence of laccase. A slightly broadening

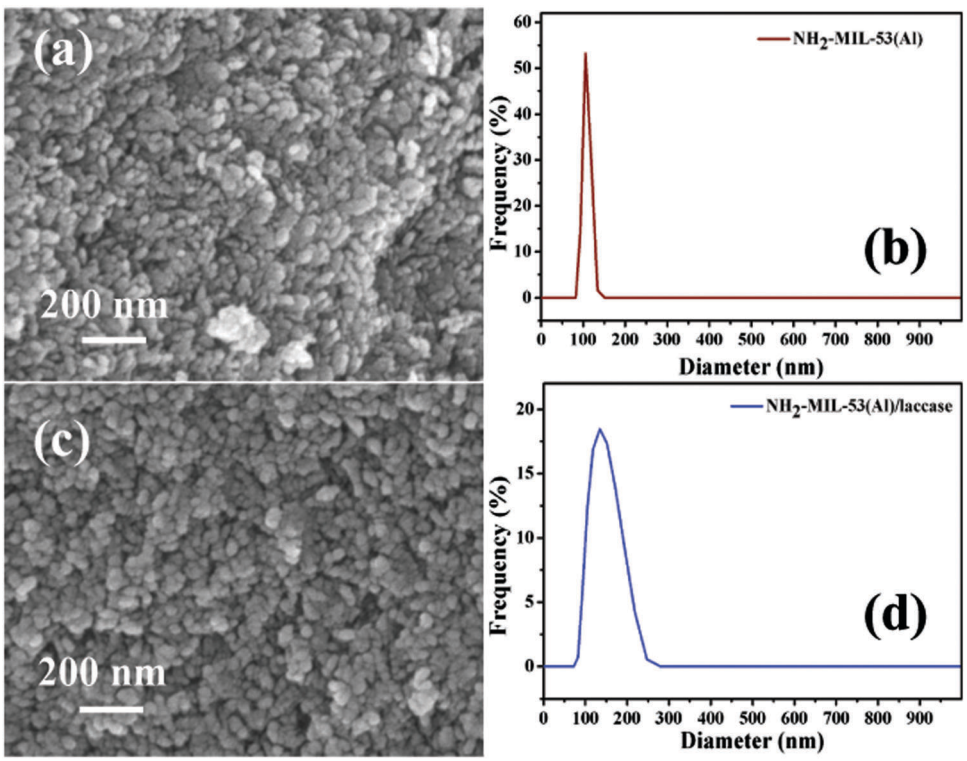

Fig. 1 FESEM images of (a) NMOF and (c) NMOF–laccase composite; DLS spectra of (b) NMOF and (d) NMOF–laccase composite.

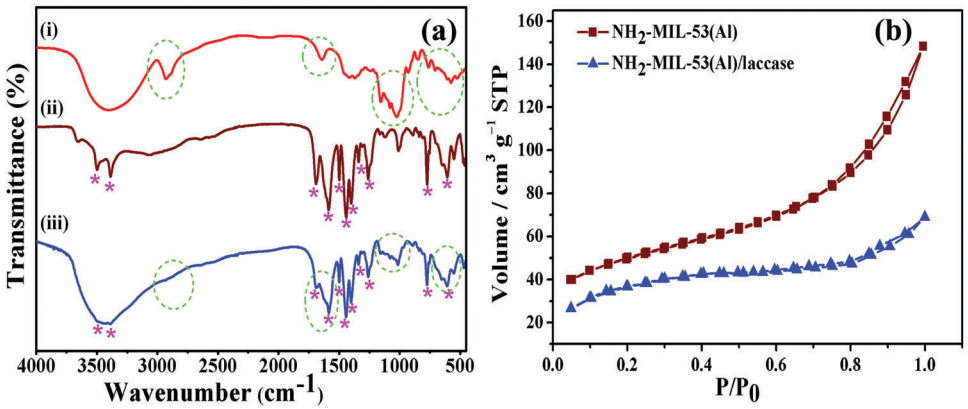

Fig. 2 (a) FTIR image of (i) laccase, (ii) NMOF, and (iii) NMOF–laccase composite; (b) nitrogen adsorption–desorption isotherm of NMOF and NMOF–laccase composite.

of the amide I peak at around 1642 cm^{-1} was observed compared with that in pure NMOF, and of the amide V and VI peaks at 800–500 cm^{-1}. All other laccase peaks, such as protein peaks (1165–948 cm^{-1}), were also present in NMOF–laccase composites. There, FTIR analysis showed that laccase was successfully immobilized into the NH_2-MIL-53(Al) structure, with both the enzyme and NMOF remaining intact.

3.3. Surface area analysis

Laccase immobilization into the NMOF using this one pot synthetic procedure was further confirmed by analyzing the surface area and pore size of both NH_2-MIL-53(Al) and NH_2-MIL-53(Al)/laccase. Microporous BET analysis was performed to determine the surface area of both the NMOF and NMOF–laccase composite, as shown in Fig. 2b and Table 1. The surface area of the NMOF was found to be 345.8 $m^2\ g^{-1}$. The high surface area of NMOFs leads to a high amount of enzyme loading.[49] After enzyme loading, the surface area of NH_2-MIL-53(Al)/laccase was observed 116.1 $m^2\ g^{-1}$. Therefore, it can be concluded that the laccase was loaded into the NMOF, leading to a decrease in surface area. As MOFs are generally porous, laccase immobilization should affect the NMOF pore width. The pore diameter of the NMOF was 0.545 nm, which decreased to 0.277 nm after laccase immobilization. This decrease in pore width was due to the NMOF pores being blocked by laccase.

3.4. XRD analysis

The framework structure and phase purity of the NMOF and NMOF–laccase composite were identified by XRD analysis, as shown in Fig. 3a. In the XRD spectrum of NH_2-MIL-53(Al), typical peaks at $2\theta = 10.4^\circ$, 15.0°, 17.4°, and 26.4° were consistent with the simulated XRD spectrum of MIL-53as.[50] However, these peaks were slightly broader than those reported in the literature, where MOFs were prepared at high temperature. This might be due to NMOF having a smaller particle size,[39] but with the crystalline structure retained. After one-pot laccase immobilization into NH_2-MIL-53(Al), the XRD spectrum was almost identical to that of the bare NMOF and the simulated spectrum. No extra peaks were generated and no peak positions were shifted after enzyme immobilization. This indicated that the NMOF–laccase composite had the same phase purity as the simulated structure. However, the intensity of some peaks varied after immobilization, such as the peak at 12.3°, which was diminished, and the peaks at 21.15° and 23.68°, which were more intense. These changes might be due to laccase immobilization. Therefore, the XRD patterns indicated that the phase purity and crystalline structure of the NH_2-MIL-53(Al) framework were retained after laccase immobilization.

Table 1 BET surface area and pore size of NMOF and NMOF–laccase composite

Material	BET surface area ($m^2\ g^{-1}$)	Pore diameter (nm)
NH_2-MIL-53(Al)	345.8	0.545
NH_2-MIL-53(Al)/laccase	116.1	0.277

3.5. TGA analysis

The thermal behavior of the NMOF and NMOF–laccase composite was analyzed by thermogravimetric analysis, as shown in Fig. 3b. The TG curve of the NMOF showed an initial gradual weight loss from 85 °C due to the desorption of water present inside the NMOF pores. The major weight loss (almost 28%) of the NMOF occurred at 420–617 °C due to the decomposition of organic ligand NH_2-BDC.[44] The TG curve of the NMOF–laccase composite showed a three-stage weight loss. Firstly, slight weight loss (almost 4%) was observed at 80–86 °C due to water desorption. A second weight loss (almost 15%) was observed at 100–345 °C, including a sharp weight loss at 300 °C, which was attributed to laccase decomposition *via* carbonization or degradation at 100–300 °C, in agreement with previous reports.[22,38] The third weight loss (almost 30%) occurred at 425–617 °C due to decomposition of the NMOF precursors. Comparing the TG curves of the NMOF and NMOF–laccase composite showed that the first weight loss of the pure NMOF was higher than that of the NMOF–laccase composite. In the composite, laccase is immobilized into the pores of the NMOF. But for pure NMOF there is no laccase present, so pore of the NMOF is filled with water molecule and rate of evaporation of water is higher than the laccase as temperature increased. Therefore, below 345 °C, the weight loss of the NMOF–laccase composite was lower than that of the pure NMOF. Above 345 °C, both showed the same weight loss rate. The TGA showed that

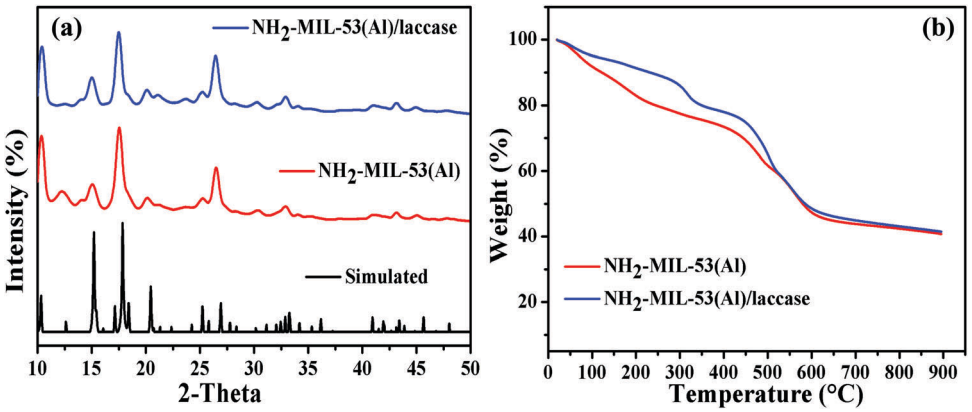

Fig. 3 (a) X-ray diffraction pattern of NH_2-MIL-53(Al), NH_2-MIL-53(Al)/laccase, and the simulated structure;[50] (b) TGA thermogram of the NMOF and NMOF–laccase composite.

laccase was successfully immobilized into the NMOF and that immobilization did not affect the thermal behavior of the NMOF.

3.6. Effect of pH

The effect of pH on free and immobilized laccase was studied, as shown in Fig. 4b. At pH 3, both free and immobilized laccase showed maximum activity. As the pH was increased, the activities of both free and immobilized laccase decreased, but with the immobilized laccase showing greater activity than that of free laccase at each pH value. The laccase activity decrease with changing pH has two possible explanations: (i) the enzyme might be denatured at a higher pH, or (ii) the higher pH might dissociate the enzyme active sites. Free laccase possessed maximum activity under acidic conditions (pH 3.0). However, the NMOF synthesized in this study contained amine functional groups. Therefore, the NMOF might absorb H^+ ions from the buffer solution and make the surface more acidic than the buffer solution. For this reason, the activity of immobilized laccase was higher than that of free laccase at the same pH.[38,40]

3.7. Effect of temperature study

The effect of temperature on free and immobilized laccase was examined, as shown in Fig. 4b. At 30 °C, both free and immobilized laccase possessed maximum activity, which

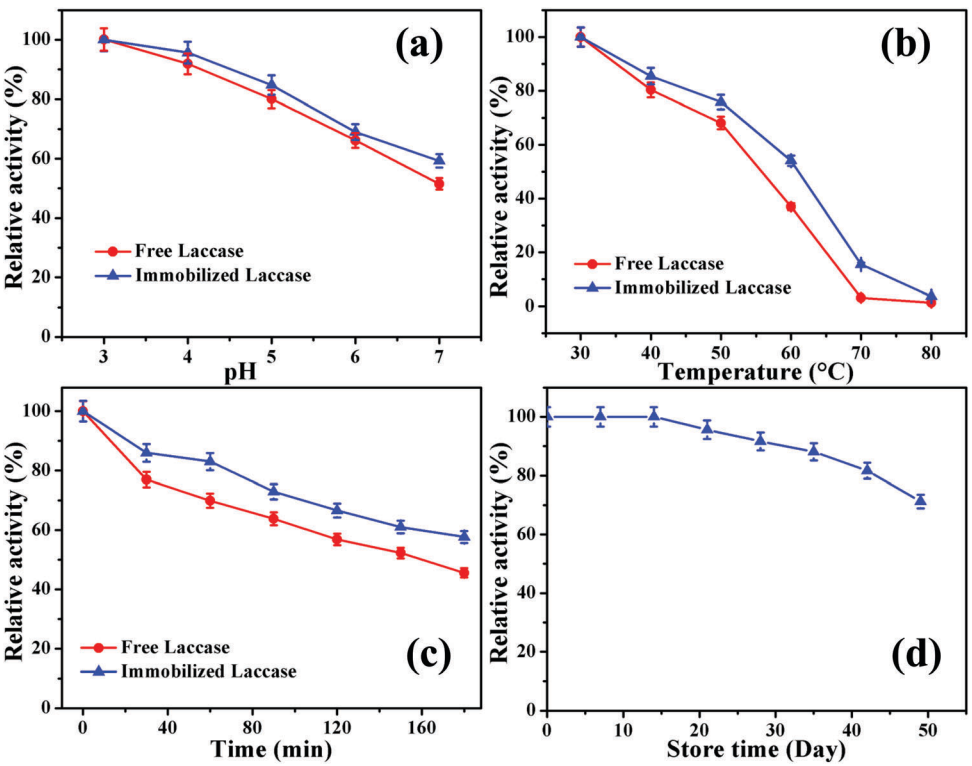

Fig. 4 Effect of (a) pH and (b) temperature on free and immobilized laccase; (c) thermal stabilities of free and immobilized laccase at 60 °C; (d) storage stability of immobilized laccase.

diminished as the temperature increased. At 50 °C, free laccase showed 68% of its initial activity, while immobilized laccase activity was at 76%. With increasing temperature, the immobilized laccase showed significantly improved enzymatic activity. This improvement might be due to the multiple linkages between the support and enzyme, through which laccase is attached to the microporous NMOF, leading to a stable conformation. In contrast, free laccase undergoes conformational changes as the temperature increases, resulting in activity decreasing at a faster rate than that of the immobilized laccase.[33,40,51]

3.8. Thermal stability study

The thermal stabilities of free and immobilized laccase were compared at 60 °C, as shown in Fig. 4c. The activity of both free and immobilized laccase decreased with increasing time. However, the relative activity of immobilized laccase remained higher than that of free laccase at each time interval. After 3 h, free and immobilized laccase retained 45% and 58% of their initial activities, respectively. After immobilization, the enzyme was attached to the microporous NMOF, which inhibited changes in conformation and reduced molecular mobility. Therefore, the thermal stability of laccase increased after immobilization into the NMOF.[40]

3.9. Storage stability study

The storage stability of the immobilized laccase plays a significant role in retaining its enzyme activity. Therefore, immobilized laccase was stored at 4 °C and its activity measured at fixed time intervals to determine the storage stability. The stability graph is shown in Fig. 4d. After 49 days, 72% of the initial activity of immobilized laccase was retained. This satisfactory storage stability suggested that multiple linkages between the enzyme and support were present, which prevented enzyme denaturation or leaching from the support.[22,40]

3.10. Kinetic study

To determine the catalytic efficiency of free and immobilized laccase, kinetic parameters (Michaelis–Menten constant (K_m), and maximum rate of reaction (V_{max})) were calculated using Michaelis–Menten and Lineweaver–Burk plots, as shown in Fig. 5. K_m represents the substrate concentration at which the reaction rate is half the maximum value. Therefore, when the enzyme has a small K_m value, it achieves maximum catalytic efficiency at a low substrate concentration, which indicates that the enzyme has high catalytic efficiency. The K_m and V_{max} values for free laccase and NH_2-MIL-53(Al)/laccase were calculated and are summarized in Table 2. The K_m value after one-pot laccase immobilization was higher than that of free laccase. Therefore, after laccase immobilization, the substrate affinity decreased compared with that of free laccase. The K_m and V_{max} values are compared with those reported elsewhere in Table S4 (ESI†). The slight decrease in affinity between substrate ABTS and immobilized laccase might be due to diffusional limits. The enzyme is immobilized into the pores of the microporous NMOFs through multipoint linkages, which decreases enzyme flexibility. As a result, structural changes in the enzyme active sites are inhibited after immobilization, which is necessary for optimal enzyme–substrate binding.[33,40,52,53] Therefore, the catalytic efficiency of NH_2-MIL-53(Al)/laccase was lower than that of free laccase. The V_{max} value for both free and immobilized laccase remained similar. Therefore, laccase immobilization into the NMOF had a small effect on the rate of catalysis.

3.11. Reusability study

Reusability is a key in enzyme immobilization. For industrial applications, both good catalytic activity and preservation are important criteria for enzyme immobilization. After one-pot laccase immobilization, the catalyst reusability was studied, as shown in Fig. 6a. The activity of immobilized laccase decreased gradually after three cycles during reusability tests. As the laccase was immobilized into the pore and surface of the NMOF, the configuration of enzyme may be changed which leads to denaturation of enzyme. The immobilized enzyme might also be leached out from the NMOF surface. For these two reasons, the laccase

Table 2 Kinetic parameters of free and immobilized laccase

	K_m (mM mL^{-1})	V_{max} (mM mg^{-1} min^{-1})
Free laccase	0.545	0.4418
Immobilized laccase	0.8037	0.4765

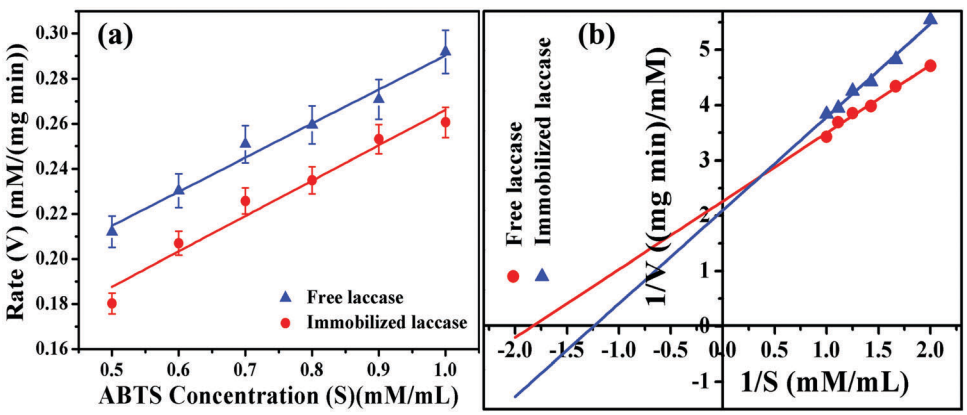

Fig. 5 (a) Michaelis–Menten plots and (b) Lineweaver–Burk plots of free and immobilized laccase.

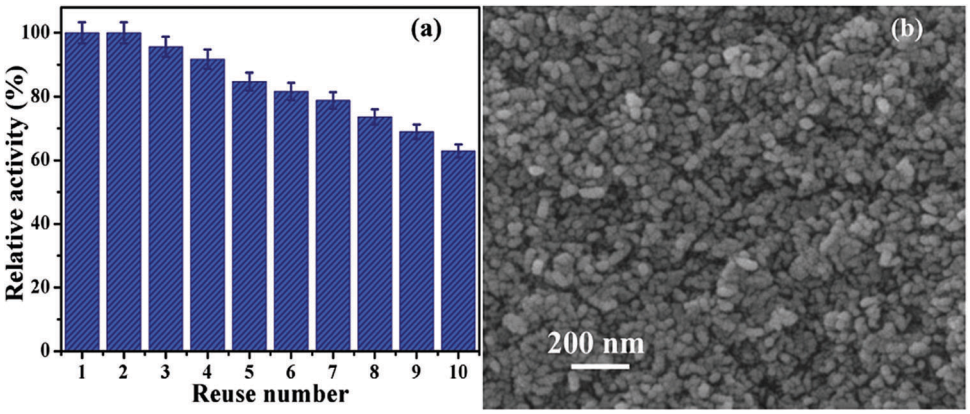

Fig. 6 (a) Reusability graph of immobilized laccase; (b) FESEM image of NMOF after reuse.

activity decreased gradually.[22,33] The results showed that the immobilized laccase retained 63% of its initial activity after 10 reuse cycles. Therefore, immobilized laccase was concluded to have good reusability.[22] The effect of reuse 10 times on the morphology was observed by FESEM of NH_2-MIL-53(Al)/laccase, as shown in Fig. 6b, which showed no change in morphology.

4. Conclusion

In conclusion, we have successfully developed an amine-functionalized NMOF with high surface area for enzyme immobilization in aqueous medium. The synthesized NMOF was stable at low pH, which is essential for laccase immobilization. Morphological studies of the NMOF indicated that size and shape was similar after enzyme immobilization using a one-pot process. From the BET analysis it can conclude that laccase is entrapped in the pore of the NMOF because after immobilization pore size of the NMOF is decreased. Immobilized laccase showed better pH stability and thermal stability than free laccase. The synthesized NMOF might be used for the immobilization of other enzymes.

Conflicts of interest

There are no conflicts to declare.

Acknowledgements

The authors thank the Indian Institute of Technology (ISM) Dhanbad for providing funding for this research.

References

1 R. DiCosimo, J. McAuliffe, A. J. Pouloseb and G. Bohlmann, *Chem. Soc. Rev.*, 2013, **42**, 6437–6474.
2 V. L. Sirisha, A. Jain and A. Jain, *Adv. Food Nutr. Res.*, 2016, **79**, 179–211.
3 M. C. R. Franssen, P. Steunenberg, E. L. Scott, H. Zuilhof and J. P. M. Sanders, *Chem. Soc. Rev.*, 2013, **42**, 6491–6533.
4 Z. Zhou and M. Hartmann, *Chem. Soc. Rev.*, 2013, **42**, 3894–3912.
5 P. Jochems, Y. Satyawali, L. Diels and W. Dejonghe, *Green Chem.*, 2011, **13**, 1609–1623.
6 E. P. Cipolatti, A. Valério, R. O. Henriques, D. E. Moritz, J. L. Ninow, D. M. G. Freire, E. A. Manoel, R. Fernandez-Lafuente and D. de Oliveira, *RSC Adv.*, 2016, **6**, 104675–104692.
7 T. K. Mahto, A. Ray Chowdhuri, B. Sahoo and S. K. Sahu, *Polym. Compos.*, 2016, **37**(4), 1152–1160.
8 S. Wuttke, M. Lismont, A. Escudero, B. Rungtaweevoranit and W. J. Parak, *Biomaterials*, 2017, **123**, 172–183.
9 M. Lismont, L. Dreesen and S. Wuttke, *Adv. Funct. Mater.*, 2017, **27**, 1606314.
10 H. Furukawa, K. E. Cordova, M. O'Keeffe and O. M. Yaghi, *Science*, 2013, **341**, 1230444.
11 A. Ray Chowdhuri, B. Das, A. Kumar, S. Tripathy, S. Roy and S. K. Sahu, *Nanotechnology*, 2017, **28**, 095102.
12 A. Ray Chowdhuri, T. Singh, S. K. Ghosh and S. K. Sahu, *ACS Appl. Mater. Interfaces*, 2016, **8**, 16573–16583.
13 X. Lian, Y. Fang, E. Joseph, Q. Wang, J. Li, S. Banerjee, C. Lollar, X. Wang and H. C. Zhou, *Chem. Soc. Rev.*, 2017, **46**, 3386–3401.
14 E. Gkaniatsou, C. Sicard, R. Ricoux, J. P. Mahy, N. Steunou and C. Serre, *Mater. Horiz.*, 2017, **4**, 55–63.
15 A. Samui, A. Ray Chowdhuri, T. K. Mahto and S. K. Sahu, *RSC Adv.*, 2016, **6**, 66385–66393.
16 Y. Cao, Z. Wu, T. Wang, Y. Xiao, Q. Huo and Y. Liu, *Dalton Trans.*, 2016, **45**, 6998–7003.
17 S. L. Cao, D. M. Yue, X. H. Li, T. J. Smith, N. Li, M. H. Zong, H. Wu, Y. Z. Ma and W. Y. Lou, *ACS Sustainable Chem. Eng.*, 2016, **4**, 3586–3595.
18 K. Wang, N. Li, J. Zhang, Z. Zhang and F. Dang, *Biosens. Bioelectron.*, 2017, **87**, 339–344.
19 C. Tudisco, G. Zolubas, B. Seoane, H. R. Zafarani, M. Kazemzad and J. Gascon, *RSC Adv.*, 2016, **6**, 108051–108055.
20 M. B. Majewski, A. J. Howarth, P. Li, M. R. Wasielewski, J. T. Hupp and O. K. Farha, *CrystEngComm*, 2017, **19**, 4082–4091.
21 K. Liang, C. J. Coghlan, S. G. Bell, C. Doonan and P. Falcaro, *Chem. Commun.*, 2016, **52**, 473–476.
22 S. Pang, Y. Wu, X. Zhang, B. Li, J. Ouyang and M. Ding, *Process Biochem.*, 2016, **51**, 229–239.

23 C. Hou, Y. Wang, Q. Ding, L. Jiang, M. Li, W. Zhu, D. Pan, H. Zhu and M. Liu, *Nanoscale*, 2015, **7**, 18770–18779.
24 X. Wu, J. Ge, C. Yang, M. Hou and Z. Liu, *Chem. Commun.*, 2015, **51**, 13408–13411.
25 S. S. Nadar and V. K. Rathod, *Int. J. Biol. Macromol.*, 2017, **95**, 511–519.
26 M. M. Rodríguez-Delgado, G. S. Alemán-Nava, J. M. Rodríguez-Delgado, G. Dieck-Assad, S. O. Martínez-Chapa, D. Barceló and R. Parra, *Trends Anal. Chem.*, 2015, **74**, 21–45.
27 S. R. Couto and J. L. T. Herrera, *Biotechnol. Adv.*, 2006, **24**, 500–513.
28 T. Kudanga, G. S. Nyanhongo, G. M. Guebitz and S. Burton, *Enzyme Microb. Technol.*, 2011, **48**, 195–208.
29 J. R. Jeon and Y. S. Chang, *Trends Biotechnol.*, 2013, **31**(6), 335–341.
30 A. A. Abd El Aty, F. A. Mostafa, M. E. Hassan, E. R. Hamed and M. A. Esawy, *Biocatal. Agric. Biotechnol.*, 2017, **9**, 74–81.
31 C. Ji, L. N. Nguyen, J. Hou, F. I. Hai and V. Chen, *Sep. Purif. Technol.*, 2017, **178**, 215–223.
32 J. Dai, H. Wang, H. Chi, Y. Wang and J. Zhao, *J. Environ. Chem. Eng.*, 2016, **4**, 2585–2591.
33 S. Rouhani, A. Rostami and A. Salimi, *RSC Adv.*, 2016, **6**, 26709–26718.
34 J. Lin, Q. Wen, S. Chen, X. Le, X. Zhou and L. Huang, *Int. J. Biol. Macromol.*, 2017, **96**, 377–383.
35 R. A. Fernandes, A. L. Daniel-da-Silva, A. P. M. Tavares and A. M. R. B. Xavier, *Chem. Eng. Sci.*, 2017, **158**, 599–605.
36 R. Chandra and P. Chowdhary, *Environ. Sci.: Processes Impacts*, 2015, **17**, 326–342.
37 Y. Lin and P. M. Lloyd, *J. Chem. Educ.*, 2006, **83**(4), 638–640.
38 Z. Zhong, S. Pang, Y. Wu, S. Jiang and J. Ouyang, *J. Chem. Technol. Biotechnol.*, 2017, **92**(7), 1841–1847.
39 M. Sánchez-Sánchez, N. Getachew, K. Díaz, M. Díaz-García, Y. Chebude and I. Díaz, *Green Chem.*, 2015, **17**, 1500–1509.
40 G. Li, A. G. Nandgaonkar, K. Lu, W. E. Krause, L. A. Lucia and Q. Wei, *RSC Adv.*, 2016, **6**, 41420–41427.
41 G. Li, A. G. Nandgaonkar, Q. Wang, J. Zhang, W. E. Krause, Q. Wei and L. A. Lucia, *J. Membr. Sci.*, 2017, **525**, 89–98.
42 A. Ray Chowdhuri, D. Laha, S. Pal, P. Karmakar and S. K. Sahu, *Dalton Trans.*, 2016, **45**, 18120–18132.
43 R. Abedini, M. Omidkhah and F. Dorosti, *RSC Adv.*, 2014, **4**, 36522–36537.
44 X. Cheng, A. Zhang, K. Hou, M. Liu, Y. Wang, C. Song, G. Zhange and X. Guo, *Dalton Trans.*, 2013, **42**, 13698–13705.
45 K. Kato, K. Inukai, K. Fujikura and T. Kasuga, *New J. Chem.*, 2014, **38**, 3591–3599.
46 F. Li, Z. Li, C. Zeng and Y. Hu, *J. Braz. Chem. Soc.*, 2017, **28**(6), 960–966.
47 J. Kong and S. Yu, *Acta Biochim. Biophys. Sin.*, 2007, **39**(8), 549–559.
48 P. Valle-Vigón and A. B. Fuertes, *RSC Adv.*, 2011, **1**, 1756–1762.
49 A. Ray Chowdhuri, D. Laha, S. Chandra, P. Karmakar and S. K. Sahu, *Chem. Eng. J.*, 2017, **319**, 200–211.
50 T. Loiseau, C. Serre, C. Huguenard, G. Fink, F. Taulelle, M. Henry, T. Bataille and G. Férey, *Chem. – Eur. J.*, 2004, **10**, 1373–1382.
51 S. K. S. Patel, V. C. Kalia, J. H. Choi, J. R. Haw, I. W. Kim and J. K. Lee, *J. Microbiol. Biotechnol.*, 2014, **24**(5), 639–647.
52 J. Lin, Y. Liu, S. Chen, X. Le, X. Zhou, Z. Zhao, Y. Ou and J. Yang, *Int. J. Biol. Macromol.*, 2016, **84**, 189–199.
53 T. Preiß, A. Zimpel, S. Wuttke and J. O. Rädler, *Materials*, 2017, **10**, 216.

